A New Critical Dimension Metrology for Chrome-on-Glass Substrates Based on S-Parameter Measurements Extracted from Coplanar Waveguide Test Structures†

Chidubem A. Nwokoye[‡a], Mona Zaghloul[a], Michael W. Cresswell[b], Richard A. Allen[b], Christine E. Murabito[b]

[a]Department of Electrical and Computer Engineering, George Washington University, Washington DC, USA, 20052-0001;

[b]Semiconductor Electronics Division, Electronics and Electrical Engineering Laboratory, National Institute of Standards and Technology, Gaithersburg, MD, USA 20899-8120

ABSTRACT

The technical objective of the work reported here is to assess whether radio-frequency (RF) measurements made on co-planar waveguide (CPW) test structures, which are replicated in conducting material on insulating substrates, could be employed to extract the critical dimension (CD) of the signal line using its center-to-center separation from the ground-lines as a reference. The specific near-term objective is to assess whether this CPW-based CD-metrology has sensitivity and repeatability competitive with the other metrology techniques that are now used for chrome-on-glass (COG) photomasks. An affirmative answer is encouraging because advancing to a non-contact and non-vacuum implementation would then seem possible for this application. Our modeling of specific cases shows that, when the pitch of the replicated lines of the CPW is maintained constant, the sensitivity of its characteristic impedance to the CDs of the signal and ground lines is approximately 60 Ω/µm. This is a potentially useful result. For the same implementation, the quantity $\partial C/\partial w$ has a value of approximately 45 (pF/m)/µm, which appears to be large enough to provide acceptable accuracy.

Keywords: photomask, CD metrology, S-parameters, co-planar waveguide, test structure

1. BACKGROUND AND OBJECTIVE

In photomask mask fabrication, critical dimension (CD) metrology is typically conducted by optical transmission, Scanning Electron Microscopy (SEM), and Atomic Force Microscopy (AFM) tools. These have different advantages and limitations. A metrology implementation that is not so widely known as these three techniques is electrical CD (ECD) metrology, a variation of which is the subject of this paper. There are prior reports on the extraction of geometrical information from the features of test structures replicated on chrome-on-glass (COG) masks by electrical means. For example, one approach was to probe electrical test structures that were patterned in chrome and were then tested in a dc mode.[1] In the cited report, an important innovation was providing for the electrical-length shortening of the bridge of a test structure that was configured as a micro-potentiometer. There were provisions in the test-structure design for the extraction of a parameter named δL that characterized the micro-geometry of the intersection of two features. The V/I values of the two segments of the bridge of the micro-potentiometer were extracted with Kelvin voltage taps, which enabled managing the effect of contact resistance.[2] The measured resistance values of the bridge were then used to estimate the center-to-center separations of parallel features serving as voltage taps to the bridge more accurately than had been otherwise possible as a result of correcting the physical length of each segment of the bridge

‡ dubem@gwu.edu; phone 301-946-0656; fax 301-975-5668; nist.gov

Photomask Technology 2006, edited by Patrick M. Martin, Robert J. Naber,
Proc. of SPIE Vol. 6349, 634946, (2006) · 0277-786X/06/$15 · doi: 10.1117/12.686706

with the measured δL value. Several papers subsequently reported improvements in the design and performance of electrically based feature-placement metrology and its application to COG masks.[3] Even more recently, others have applied ECD metrology to COG features of photo-plates.[4] Cross-bridge test structures were designed to allow the on-mask measurement of dense and isolated features of both phase-shift and binary masks. The comparison of electrical and CD Scanning Electron Microscope (SEM) testing of these structures indicated the lower variability of ECD measurements. The adverse effect of phase-shifting element architectures on the accuracy of SEM measurements was reported.

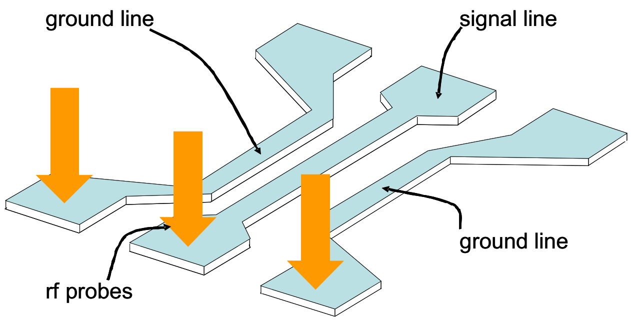

Figure 1. A CPW for the COG application shown in schematic form for radio-frequency (RF) measurements.

Although ECD provides a highly repeatable measurement, its drawback is that electrical access to the test structure by probe-card contact to the structures' test pads can sometimes generate particulate contamination. An approach to CD extraction through non-contact electrical measurements has been reported by Nadine Guillaume *et al.*[5] The principle was extracting the CDs of parallel features patterned as a grating from a measurement of the capacitance between the grating and a parallel plate that served as a sensor at relatively low ac frequencies. In the cited case, the sensor was fabricated with a co-fired low temperature ceramic technology. Although it was a non-contact method, which potentially sidestepped the particulate contamination problem, we do not know if it will become sufficiently repeatable for high-throughput metrology of sub-micrometer features. Given this situation, we decided to make a preliminary investigation into CD-metrology based on co-planar waveguide (CPW) implementation partly because it appears that it could be developed into a non-contact method. The specific near-term objective is to make an exploratory assessment of whether this CPW-based CD-metrology has sensitivity and repeatability for chrome-on-glass (COG) photomask applications.

2. CPW BASICS: EXTRACTING CHARACTERISTIC IMPEDANCE AND DISTRIBUTED CAPACITANCE FROM S-PARAMETER MEASUREMENTS

A coplanar waveguide consists of a strip of thin metallic film on the surface of a dielectric slab with two ground electrodes running adjacent and parallel to the strip. Practical applications of the coplanar waveguide have been experimentally demonstrated by others with measurements on resonant isolators and differential phase shifters fabricated on low-loss dielectric substrates with high dielectric constants.[6]

The fundamentals of a basic CPW architecture consistent with the COG application are shown schematically in Figure 1.[§] Arora *et al.*[7] have reported the use of CPW test structures for investigating the radio-frequency (RF) impedances of on-chip interconnect features having various architectures. In the implementation proposed here, which follows the Arora approach, the first task is to measure the S-parameters, S_{11}, S_{12}, S_{21}, and S_{22}, of the as-replicated CPW test structure with a network analyzer and compute from the measurements the CPW's characteristic impedance Z and its propagation constant γ. For a uniform waveguide of length l, these are given by

$$e^{-\gamma l} = \left(\frac{1 - S_{11}{}^2 + S_{21}{}^2}{2S_{21}} \pm K \right)^{-1} \qquad \text{Eq. (1)}$$

where

§ With regard to Figure 1, the illustration is schematic for illustrative purposes. What is shown is a CPW test structure, which consists of an extended waveguide having length-wise geometrical uniformity, which is terminated by end structures that include the test pads.

$$K = \left(\frac{\left(S_{11}{}^{2} - S_{21}{}^{2} + 1\right)^{2} - \left(2S_{11}\right)^{2}}{\left(2S_{21}\right)^{2}} \right)^{\frac{1}{2}} \qquad \text{Eq. (2)}$$

and

$$Z^{2} = Z_{0}{}^{2} \left(\frac{\left(1 + S_{11}\right)^{2} - S_{21}{}^{2}}{\left(1 - S_{11}\right)^{2} - S_{21}{}^{2}} \right). \qquad \text{Eq. (3)}$$

In Eq. (3), Z_0 is the termination impedance of the CPW.[8] From Z and γ, the distributed transmission-line parameters resistance R, conductance G, inductance L, and capacitance C, can be calculated according to the identities $R = \mathrm{Re}\{\gamma Z\}$, $L = \mathrm{Im}\{\gamma Z\}/\omega$, $G = \mathrm{Re}\{\gamma / Z\}$, and $C = \mathrm{Im}\{\gamma / Z\}/\omega$.

Arora *et al.*[7] used these so-called Telegrapher's equations to determine the resistance and inductance per unit length of a selection of interconnect-line implementations over frequencies ranging from 10 GHz to 50 GHz. Our approach uses the same microwave-engineering mathematics to extract the signal and ground line's CDs by cross-referencing the measured values of characteristic impedance and distributed capacitance to a listing of their values that are derived from electro-magnetic field modeling, according to the description that follows.

3. CONFORMAL MAPPING TO DETERMINE THE ELECTRICAL PARAMETERS OF THE COPLANAR WAVEGUIDE

Figure 2 shows the essential dimensions of a cross section of the general coplanar waveguide test structure that has been illustrated schematically in Figure 1. In this case, it consists of three strip lines patterned in the absorber film of a chrome-on-glass substrate.

The conformal mapping approach is applicable for deriving expressions for electrical parameters, such as impedance and distributed capacitance, of the CPW because it supports a transverse electro-magnetic mode; *i.e.*, the propagation mode is quasi-static. Typically, quasi-static approximations are valid up to a frequency of 100 GHz.[9]

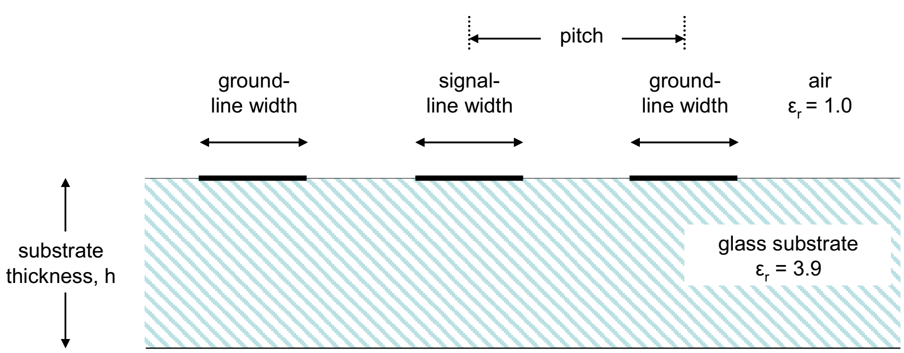

Figure 2. The essential dimensions of a cross section of the waveguide test structure that has been illustrated in Figure 1.

Since the CPW transmission line is on a single-dielectric layer, a magnetic wall can be placed on the dielectric boundary and the distributed capacitance can be partitioned into two components: that between the signal line and ground rails through the air ambient and that between the signal and ground rails through the substrate.[10]

The cross section of the CPW test structure can then be mapped into the complex z-plane, as shown in Figure 3. The first quadrant of the complex z-plane is transformed into the upper "t" half plane in Figure 5 by the mapping $t = z^2$ and then into the rectangular region of Figure 6 through the mapping

$$w = \int_{t_0}^{t} \frac{dt}{\sqrt{t(t-1)(t-t_1)(t-t_2)}}. \qquad \text{Eq. (4)}$$

In Figure 3, note that the half-linewidth of the signal line is denoted by a*,* and the gap between the near edges of the signal and ground lines is s = *b* – *a*.

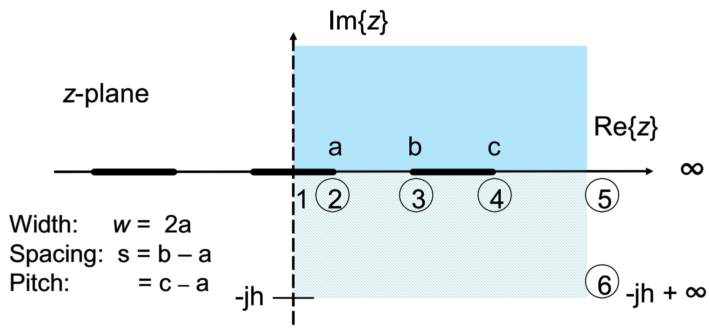

Figure 3. The cross section of the CPW test structure is mapped into a complex z-plane. (Note that the pitch is c – a only when the signal and ground lines have the same width.)

The component of the distributed capacitance between the signal line and ground rails through the air ambient then becomes[11]

$$C_0 = 4\varepsilon_0 \frac{\overline{12}}{\overline{23}} = 4\varepsilon_0 \frac{K(k)}{K(k')}. \qquad \text{Eq. (5)}$$

In Eq. (5), $\overline{ij}$ is the distance between points *i* and *j* in the *w*-plane, ε_0 is the permittivity of free space, *K* is the complete elliptical integral of the first kind, and the variables *k* and *k'* are geometrically dependent and are given by

$$k = \frac{a}{b}\sqrt{\frac{1 - b^2/c^2}{1 - a^2/c^2}} \qquad \text{Eq. (6)}$$

and

$$k' = \sqrt{1 - k^2}. \qquad \text{Eq. (7)}$$

To determine the capacitance through the substrate, the CPW representation in the z-plane is transformed into the "*x*" half-plane in Figure 4 by the mapping $x = \cosh^2(\pi z/2h)$ and then into the rectangular region in Figure 6 through the mapping

$$w = \int_{x_0}^{x} \frac{dx}{\sqrt{(x-1)(x-x_1)(x-x_2)(x-x_3)}}. \qquad \text{Eq. (8)}$$

Hence, the component of the distributed capacitance between the signal line and the ground rails can be expressed as

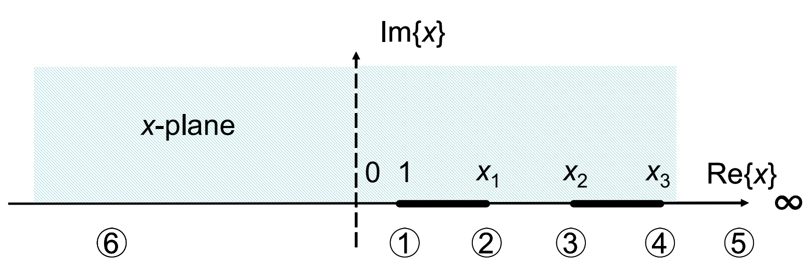

Figure 4. The shaded dielectric substrate region in the z-plane is transformed into the upper x-plane shown here through the mapping $x = \cosh^2(\pi z / 2h)$.

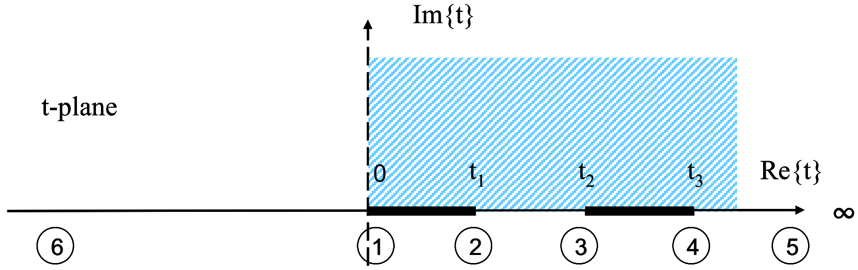

Figure 5. The first quadrant of the complex z-plane is transformed into the upper “t” half plane by the mapping $t = z^2$.

$$C_1 = 2\varepsilon \frac{\overline{12}}{\overline{23}} = 2\varepsilon_0 (\varepsilon_r - 1) \frac{K(k_1)}{K(k_1')} \quad \text{Eq. (9)}$$

where

$$k_1 = \frac{\sinh(\pi a / 2h)}{\sinh(\pi b / 2h)} \sqrt{\frac{1 - \sinh^2(\pi b / 2h) / \sinh^2(\pi c / 2h)}{1 - \sinh^2(\pi a / 2h) / \sinh^2(\pi c / 2h)}} \quad \text{Eq. (10)}$$

and ε_r is the relative dielectric constant of the substrate.

In quasi-static operation, the distributed resistance ‘R’ and conductance ‘G’ values are negligible and, hence the effective dielectric constant, velocity of propagation, and characteristic impedance of the transmission line are given by[12]

$$\varepsilon_{eff} = \frac{C_1 + C_0}{C_0} \quad \text{Eq. (11)}$$

$$V_P = \frac{c}{\sqrt{\varepsilon_{eff}}} \quad \text{Eq. (12)}$$

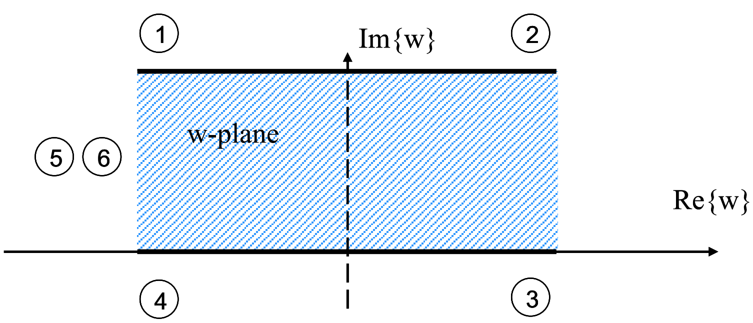

Figure 6. The distributed capacitance between the signal line and the ground rails through air and dielectric substrate are finally transformed into a plane-parallel capacitor.

and

$$Z = \sqrt{\frac{R + j\omega L}{G + j\omega C}} \cong \sqrt{\frac{L}{C}} = \frac{1}{CV_P}. \qquad \text{Eq. (13)}$$

where c is the speed of light in vacuum. The value of $C = C_0 + C_1$ embeds the value of w*,* which is the target of the measurement, according to Eqs . (5), (7), and (9), and can be extracted by available numerical methods.

4. TEST STRUCTURE LAYOUT

The layout consists of five instances of a basic cell, each of which extends over an area of approximately 0.2 mm by 11 mm. Each basic cell consists of a “thru” structure, of which the signal line is the reference feature for CD metrology, and three de-embedding structures, as shown in Figure 7. The latter have the same signal-line CD as the “thru” structure. On all structures, the signal line is between the two ground lines.

Each structure in the basic cell has a set of three 50 µm by 50 µm test pads. The connections from these pads to both the signal and ground lines taper down from the pad to optimize its electrical behavior and to reduce mechanical stress, thus minimizing the possibility of breakage. The geometries of the test-pad set are shown in Figure 8.

The “thru” structure consists of a 10.4 mm long signal line surrounded by a ground line of the same length on each side. There are two sets of test pads on a “thru” structure, one on each end of the structure. Principal dimensions of the “thru” structure are shown in Figure 9.

There are three de-embedding structures in the layout, identified as “shorted,” “loaded,” and “open.” The first two of these are shown in Figure 10 and Figure 11 respectively. The “shorted” de-embedding structure consists of a 200 µm long signal line with ground lines of the same 1 µm linewidth on either side. Each of the de-embedding structures has a probe-pad set.

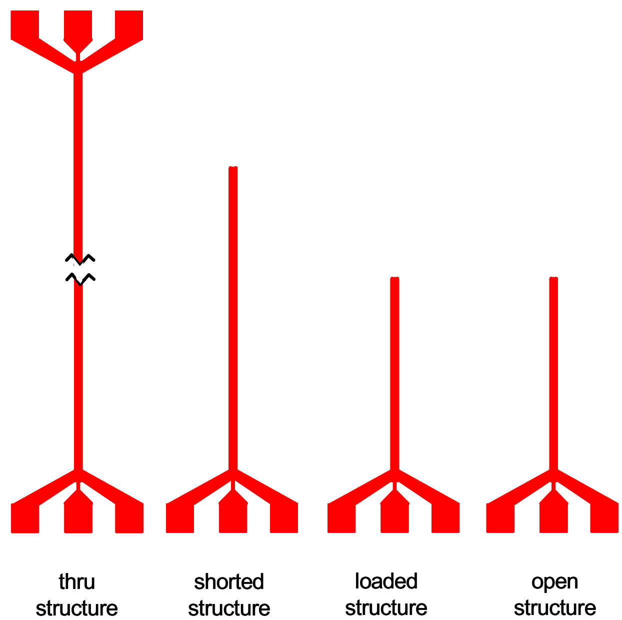

Figure 7. Each of five basic cells in the layout consists of a “thru” structure, of which the signal line is the reference feature for CD metrology, and three de-embedding structures.

On one end of the waveguide of the “shorted” structure, there is a 200 µm long box. The width of this 200 µm box extends laterally from the far edge of one ground line, past the signal line, to the far edge of the opposite ground line. The “loaded” de-embedding structure is the same as the “shorted” de-embedding structure, except that it has a 2 µm long box on one end as opposed to the 200 µm long box on the “shorted” structure. The “open” de-embedding structure has a 200 µm-long signal line surrounded by a ground line of the same length on each side. It closely resembles the layout shown in Figure 8 except that the wavwguide extends for 200 µm, as indicated in Figure 7. There is nothing on the other end of the “open” structure, leaving the signal line and the ground lines open with nothing touching them on that end of the structure.

The basic cell is replicated 5 times on the test substrate, giving a total of 20 structures in the layout. The signal and ground lines of all structures have a CD of 1.0 µm. The space between the signal line and the ground lines varies in each instance of the basic cell, ranging from 0.7 µm to 2.0 µm. The area of the composite test-structure set is approximately 15 mm by 11 mm.

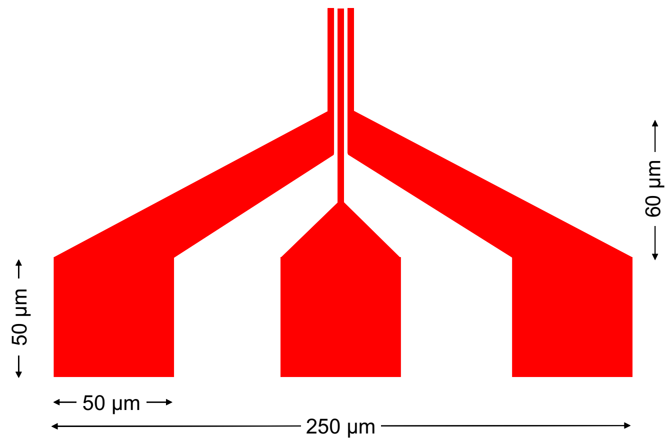

Figure 8. Each structure in the basic cell has a set of three 50 µm by 50 µm test pads, the geometries of which are shown here.

The next section shows a selection of results of field modeling of the dependence of the characteristic impedance and the distributed capacitance, respectively, on the CDs of the ground and signal lines of the CPW that has been represented in Figure 1.

5. EXAMPLES OF MODELING RESULTS

Examples of the dependence of the total distributed capacitance on the CPW's signal-line CD of w, and its separation from the inside edges of the ground lines, *s,* according to Eqs. (5) and (9), are illustrated in Figure 12, for cases in which the ground lines are attributed the same CDs as the signal line and the dielectric substrate thickness, h, is 100 µm. The capacitance values listed on the y-axis of the chart are measurable with a modern rf-

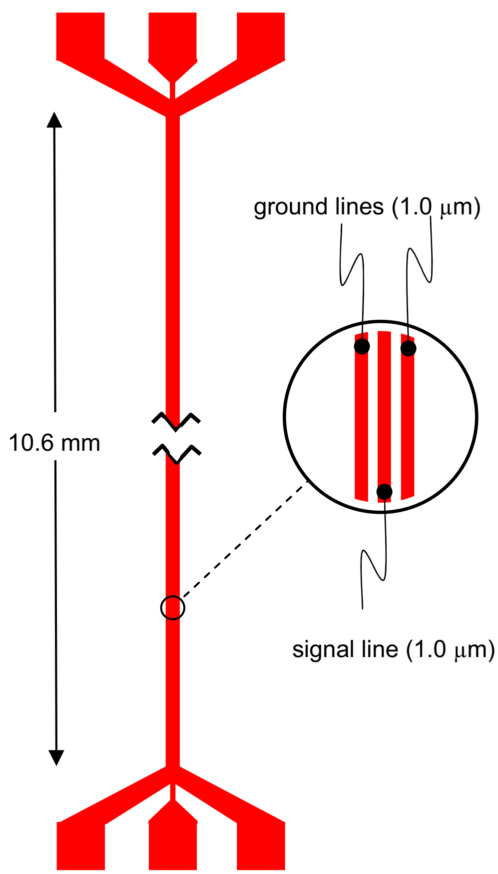

Figure 9. The "thru" structure consists of a 10.4 mm long waveguide having 1 µm wide ground and signal lines and a probe-pad set on each end.

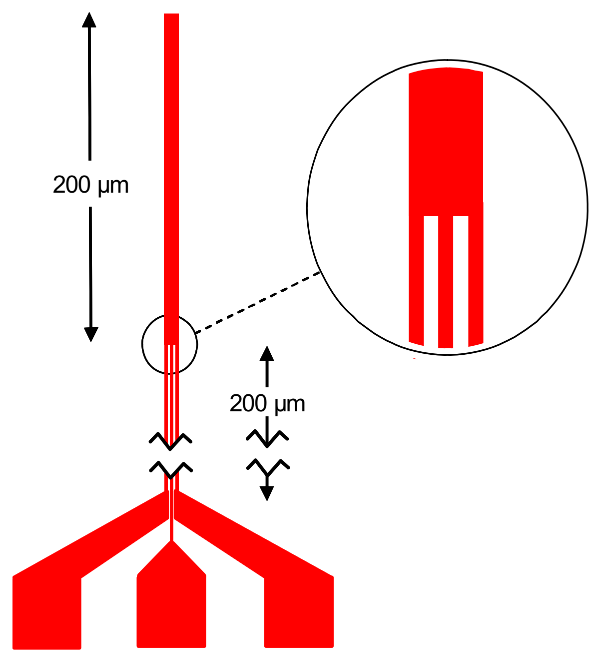

Figure 10. The "shorted" de-embedding structure consists of a 200 µm long signal line surrounded by a ground line of the same length on each side. On one end it has test pads and the other end is terminated by a 200 µm long box.

probing technique, which means that the operator should be able to obtain a nominal value of signal-line width from the value of C. The increase of distributed capacitance as w increases and s decreases is expected.

The trend line rising from the lower left to the upper right of the plot area of the chart tracks the increase of C with w when the pitch, w + s, is maintained constant. This represents what actually would happen, certainly to a good first approximation, when a CPW, having drawn ground and signal lines of equal width, is replicated on a substrate under different lithography or etch bias conditions. For this implementation, the quantity $\partial C/\partial w$ has a value of approximately 45 (pF/m)/µm when the ground and signal lines have a CD of 1.0 µm and are separated by 1.0 µm. However, this remains to be proven by further analyses of actual calibrated measurements in the future. However, it is considered highly likely that the sensitivity could be improved by incorporating the results of further simulations into the design of the CPW.

One final comment about the data points is that we processed the same dimensional inputs numerically with a Maxwell solver. The outcome was that the results for C were approximately 6 % higher than when predicted by the conformal-mapping-based results. This is clearly an issue that needs further investigation but is not at this time considered to be a showstopper with regard to the limited objective of the work being reported.

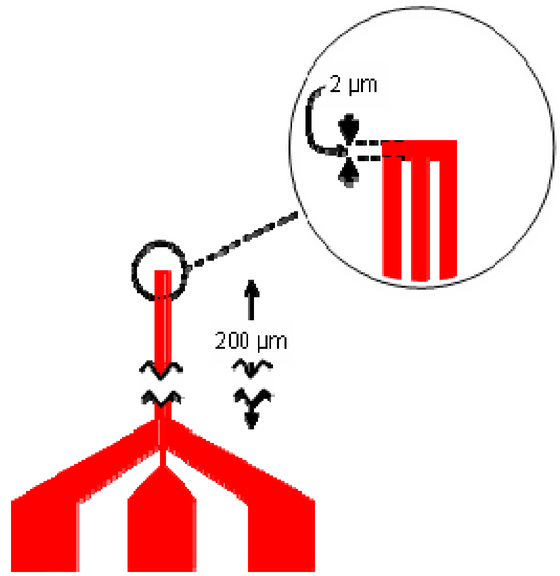

Figure 11. The "loaded" de-embedding structure is similar to the "shorted" except that the waveguide is terminated by a 2 µm line.

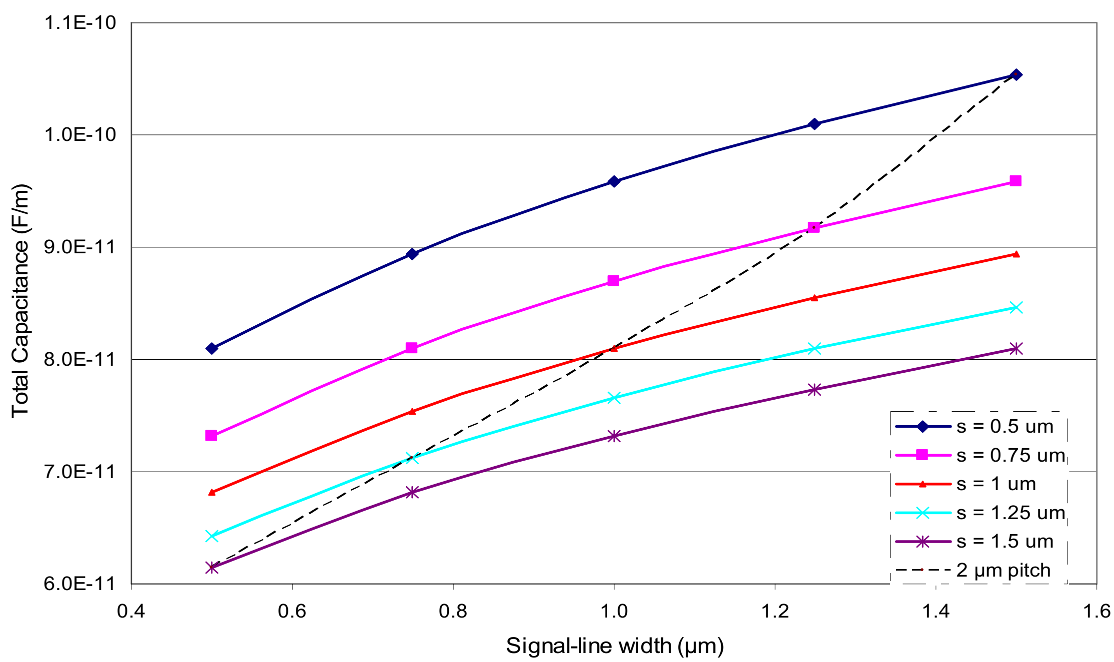

Figure 12. Examples of the dependence of values of the total distributed capacitance on the CPW's signal-line CD and its separation from the inside edges of the ground lines, s, according to Eqs. (5) and (9).

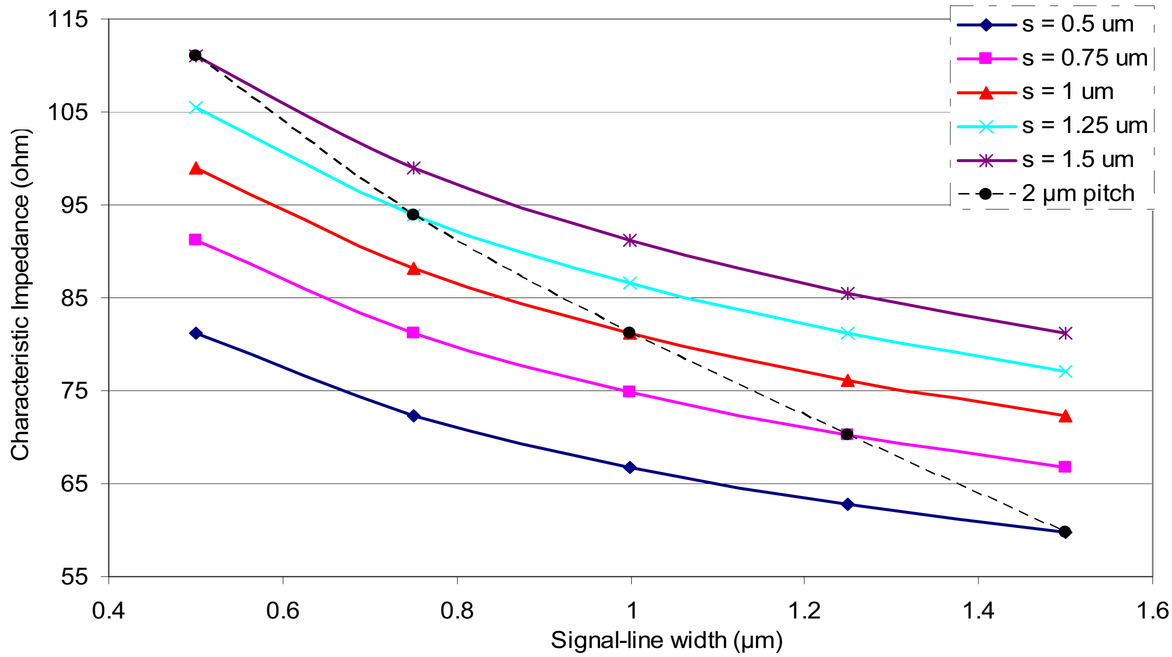

Figure 13. The conformal mapping-based simulations indicate that the characteristic impedance Z, according to Eq. (13), decreases with decreasing *s* and increasing w.

We have also observed from the conformal-mapping-based simulations that the value of the characteristic-impedance-parameter Z, according to Eq. (13), decreases as *s* decreases and w increases, as expected. Its sensitivity to CD is illustrated by the trend line decreasing from the upper left to the lower right in the plot area of the chart in Figure 13 with w when the pitch, w + s, is maintained at a constant at 2.0 µm. The sensitivity of Z to CD is approximately 60 Ω/µm when the ground and signal lines have CDs of 1.0 µm and are separated by 1.0 µm. Even though this result seems potentially more useful than that for C, it is clear that, in any implementation of this new metrology approach, co-reconciliation of the respective measured and modeled values of both C and Z might reduce the overall uncertainty of the extracted value of *w*. Similar benefits could be expected if other RF parameters such as R and L were incorporated into the linewidth-extraction analyses.

6. SUMMARY AND CONCLUSIONS

This paper describes an initial investigation of a new metrology concept for extracting critical dimensions of selected features embedded in test structures that are patterned in binary masks having absorbers of conducting material, such as in the COG implementation. It was undertaken as the prelude to an actual laboratory implementation. The test structures are coplanar waveguides, and the linewidths of their signal lines are extracted from rf measurements that are performed on them. It has the advantage of being a non-vacuum technique. The approach is to estimate the CDs of the selected feature by matching the measured characteristic impedance and distributed capacitance of the waveguide to corresponding values obtained from electromagnetic (e-m) field modeling. Our modeling of the case when the pitch of the replicated features of the CPW is 2.0 µm, and their linewidths are 1.0 µm, the sensitivity of the CPW's characteristic impedance to the linewidths is approximately 60 ohms per micrometer. This would seem to be a very encouraging result. Under the same conditions, the quantity $\partial C/\partial w$ has a value of approximately 45 pF/m/µm, which appears to be large enough to provide acceptable accuracy. However, this remains to be proven by further analyses of actual calibrated measurements in the future.

In future work, finite-element based high-frequency simulation software will be used allow parallel analyses at multiple frequencies to broaden the database from which a signal-line CD is extracted. The initial implementation, the test-structure design that has been shown here, will be patterned on binary masks. If successful, it will be extended to the examination of opportunities in dimensional metrology for more complex phase-shift mask applications. Further into the future, the experience gained here may be useful for development of a non-contact waveguide based electrical-CD metrology.

The work reported here is the disclosure and simulation of an alternative metrology for extracting critical dimensions of selected features replicated on photomasks having electrically conducting absorber patterns, which are embedded in test structures.

7. ACKNOWLEDGMENTS

The authors acknowledge the NSF Summer Undergraduate Research Fellowship program at NIST for funding that enabled this R&D effort to initiate. The authors acknowledge valued comments by the reviewers Dr. Herbert S. Bennett, Erik M. Secula, Dr. J. V. Martinez de Pinillos, and of Dr. David G. Seiler at NIST, and especially those of Professor W. K. Kahn of George Washington University. Dr. Narain Aurora of Cadence Design Systems and Bill Verzi of Agilent Technologies are acknowledged for encouraging the authors in the field of waveguide applications in VLSI fabrication. Professor Jurriaan Schmitz of the University of Twente, NL, Dr. Colin McAndrew of Motorola, and Franz Sischka of Agilent Technologies are all thanked for extended helpful technical discussions. Financial support at NIST was provided by the Office of Microelectronics Programs.

8. REFERENCES

1. M. W. Cresswell, R. A. Allen, L. W. Linholm, "A Modified Sliding Wire Potentiometer Test Structure for Mapping Nanometer-Level Distances," Proceedings of the 1991 International Conference on Microelectronic Test Structures, Vol. 4, pp. 129-134, March 1991, Kyoto, Japan.

2. Test Structures for the Electrical Characterisation of Platinum Deposited by Focused Ion Beam, S. Smith, A. J. Walton, S. Bond, A. W. S. Ross, J. T. M Stevenson, A. M. Gundlach, Proc. IEEE 2002 Int. Conference on Microelectronic Test Structures, Vol. 15, pp. 157-162, April 2002.

3. R. A. Allen, M. W. Cresswell, C. H. Ellenwood, L. W. Linholm, "The Enhanced Voltage-Dividing Potentiometer for High-Precision Feature Placement Metrology," IEEE Transactions on Instrumentation and Measurement, Vol. 45, No. 1, pp. 136-141, February 1996.

4. S. Smith, A. Tsiamis, M. McCallum, A. C. Hourd, J. T. M. Stevenson, A. J. Walton, "Comparison of Optical and Electrical Measurement Techniques for CD Metrology on Alternating Aperture Phase-Shifting Masks," Proceedings of the 2006 International Conference on Microelectronic Test Structures, Vol. 19, pp. 119-123, March 2006, Austin, Texas.

5. N. M. P. Guillaume, R. A. Allen, M. W. Cresswell, M. Lahti, L. W. Linholm, M. E. Zaghloul, "Non-contact Critical Dimension Metrology Sensor for Chrome Photomasks Featuring a Low-Temperature Co-Fired Ceramic Technology," IEEE Transactions On Semiconductor Manufacturing, Vol. 17, No. 1, pp. 25-34, February 2004.

6. C. P Wen, "Coplanar Waveguide: A Surface Strip Transmission Line Suitable for Nonreciprocal Gyromagnetic Device Applications," IEEE Transactions on Microwave Theory and Techniques, Volume: 17, No. 12, pp. 1087-1090, December 1969.

7. N. D. Arora, L. Song, S. Shah, K. Joshi, K. Thumaty, A. Fujimura, J. P. Schoellkopf, H. Brut, M. Smayling, T. Nagata, "Test Chip Characterization of X Architecture Diagonal Lines for SoC Design," Proceedings of the 2004 International Conference on Microelectronic Test Structures, Vol. 17, pp. 129-134, March 2004, Kyoto, Japan.

8. W. R. Eisenstadt, Y. Eo, "S-Parameter-Based IC Interconnect Transmission Line Characterization," IEEE Transactions On Components, Hybrids, and Manufacturing Technology, Vol. 15, No. 4, pp. 483-490, August 1992.

9. M. Y. Frankel, R. H. Voelker, J. N. Hilfiker, "Coplanar Transmission Lines on Thin Substrates for High-Speed Low-Loss Propagation," IEEE Transactions on Microwave Theory Tech., Vol. 42, No. 3, pp. 396–402, 1994.

10. R. K. Hoffmann, *Handbook of Microwave Integrated Circuit,.* Norwood, MA: Artech House, 1987.

11. G. Ghione, C. U. Naldi, "Coplanar Waveguides for MMIC Applications: Effect of Upper Shielding, Conductor Backing, Finite-Extent Ground Planes, and Line-to-Line Coupling," IEEE Transactions On Microwave Theory and Techniques, Vol. MTT-35, No. 3, pp. 260- 267, March 1987.

12. K. C. Gupta, R. Garg, I. J. Bahl, *Microstrip Lines and Slotline,.* Norwood, MA: Artech House, 1979.